AGU ADVANCING EARTH AND SPACE SCIENCE

Geophysical Research Letters

RESEARCH LETTER
10.1029/2021GL092432

Key Points:

- Reconstruction of the Arabian Sea upwelling over the past millennium based on biweekly coral records from the Arabian Sea
- Unprecedented weakening of the Arabian Sea upwelling during the current warming era
- Insignificant changes of the Arabian Sea upwelling between the medieval climate anomaly and the little ice age

Supporting Information:

Supporting Information may be found in the online version of this article.

Correspondence to:

T. Watanabe,
nabe@sci.hokudai.ac.jp

Citation:

Watanabe, T. K., Watanabe, T., Pfeiffer, M., Hu, H.-M., Shen, C.-C., & Yamazaki, A. (2021). Corals reveal an unprecedented decrease of Arabian Sea upwelling during the current warming era. *Geophysical Research Letters*, *48*, e2021GL092432. https://doi.org/10.1029/2021GL092432

Received 6 JAN 2021
Accepted 16 APR 2021

Corals Reveal an Unprecedented Decrease of Arabian Sea Upwelling During the Current Warming Era

Takaaki K. Watanabe[1,2,3], Tsuyoshi Watanabe[1,2,4], Miriam Pfeiffer[3], Hsun-Ming Hu[5], Chuan-Chou Shen[5,6], and Atsuko Yamazaki[1,2,7]

[1]Department of Natural History Sciences, Faculty of Science, Hokkaido University, Sapporo, Japan, [2]KIKAI Institute for Coral Reef Sciences, Kagoshima, Japan, [3]Institut für Geowissenschaften, Christian-Albrechts Universität zu Kiel, Kiel, Germany, [4]Research Institute for Humanity and Nature, Kyoto, Japan, [5]High-Precision Mass Spectrometry and Environment Change Laboratory (HISPEC), Department of Geosciences, National Taiwan University, Taipei, Taiwan, ROC, [6]Research Center for Future Earth, National Taiwan University, Taipei, Taiwan, ROC, [7]Department of Earth and Planetary Sciences, Faculty of Science, Kyusyu University, Fukuoka, Japan

Abstract Upwelling in the Arabian Sea driven by the Indian summer monsoon pumps deep, cold, and eutrophic seawater to the sea surface every summer. The Indian summer monsoon and the Arabian Sea upwelling were expected to intensify with global warming, following the hypothesis that the Eurasian landmass would warm faster than the Indian Ocean. Contrary to expectations, the northern Indian Ocean currently warms faster than the Indian subcontinent. A weakening of the Indian summer monsoon circulation is reported, which possibly weakens the Arabian Sea upwelling. However, a lack of observations limits understanding of current and historical changes of the Arabian Sea upwelling. Here, we reconstruct the Arabian Sea upwelling over the past millennium using modern and fossil corals. Our coral records show that the Arabian Sea upwelling intensity was very stable over the last millennium and unprecedentedly declines at present. Our finding implies anthropogenic forcing likely weakens the Arabian Sea upwelling.

Plain Language Summary The climate on the Indian Ocean is characterized by the seasonally reversing wind (Indian monsoon), driven by the difference in air temperatures between the Indian Ocean and the Indian subcontinent. During the Indian summer monsoon, strong southwesterly winds along the Arabian Peninsula push surface water away from the coast and drive the Arabian Sea upwelling. The Arabian Sea upwelling pumps cold, nutrient-rich, and low-salinity seawater to the surface and substantially impacts fisheries and weather. Originally, the Arabian Sea upwelling was expected to intensify following the hypothesis that the continent would warm faster than the Indian Ocean. Contrary to the expectations, the Indian Ocean currently warms faster than the Indian subcontinent. However, a lack of observations due to social instabilities around the Arabian Sea limits understanding of current and historical changes of Arabian Sea upwelling. Here, we reconstruct the Arabian Sea upwelling over the past millennium using modern and fossil corals collected from the Arabian Sea. Our coral archives show that the intensity of Arabian Sea upwelling was very stable over the last millennium and significantly declines at present. Our finding implies that current anthropogenic forcing (emissions of greenhouse gases and aerosols) likely weakens the Arabian Sea upwelling.

1. Introduction

The thermal contrast between the Indian subcontinent and the Indian Ocean drives the Indian monsoon circulations (Naidu et al., 2020; Roxy et al., 2015; Schott & McCreary, 2001; Wu et al., 2012). The southwest Indian monsoon (SW monsoon, Figure S1) typically peaks in boreal summer (July and August) and provides most of the total annual rainfall on the Indian subcontinent. During the SW monsoon season, strong alongshore winds along the Arabian Peninsula generate coastal upwelling in the Arabian Sea (Barber et al., 2001; Brock & McClain, 1992; Tudhope et al., 1996). The Arabian Sea upwelling pumps cold, low-salinity, and nutrient-rich water from the lower thermocline to the surface (Barber et al., 2001; Brock & McClain, 1992; Roxy et al., 2016; Tudhope et al., 1996). This cold water modulates the heat-budgets of the Arabian Sea and leads to a pronounced cooling (down to 24°C) of surface waters in the SW monsoon season (Figure S1). Upwelling-driven nutrient supply makes the Arabian Sea the highest primary productivity

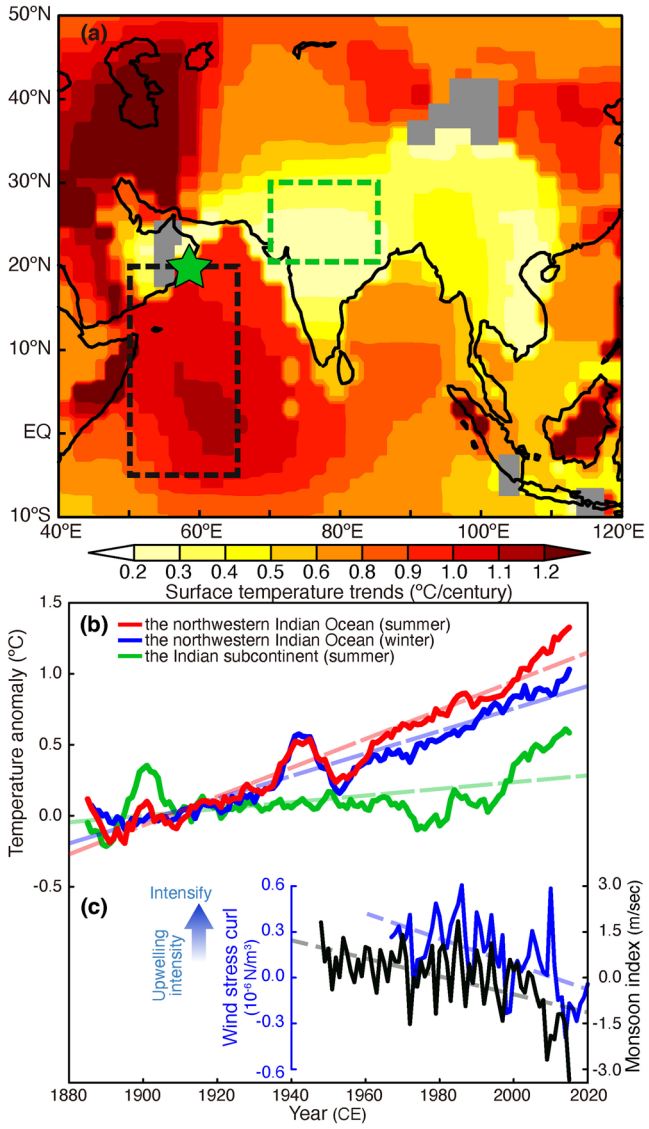

Figure 1. Warming trends of the northern Indian Ocean and the Indian subcontinent. (a) Color map of warming trends in July–September (GISS temperature, 1880–2019 CE) (Hansen et al., 2010). The star indicates the sample site of our modern and fossil Arabian Sea corals. The map is computed with the web application KNMI Climate explorer and plotted using GrADS 2.2.0. Correlations not significant at the 10% level are masked out (gray shading). (b) Anomalies of surface temperature (10-year moving averaged GISS; relative to 1880–1900 CE) in the northwestern Indian Ocean in summer and winter (red line: July–September; blue line: December–February; averaged over 5°S–20°N, 50°–65°E, black box in Figure 1a) and the central Indian subcontinent in summer (green line: July–September; averaged over 20°–30°N, 70°–85°E, green box in Figure 1a). Dashed lines show the warming trend in each region. (c) Wind stress curl (data from FNMOC; blue line) from near our sample site and the Indian summer monsoon circulation index (black line) in June–August (Webster & Yang, 1992). Dashed lines show trends of wind stress curl and the monsoon index.

ocean in the tropics. The high primary-productivity in the Arabian Sea is important for commercial fishing in the Indian Ocean (Roxy et al., 2016). The SW monsoon circulation and the Arabian Sea upwelling are a key factor for climate, ecosystems, and socioeconomics in the densely populated region surrounding the Indian Ocean (Izumo et al., 2008; Krishna Kumar et al., 2004; Roxy et al., 2016).

Originally, the SW monsoon and the Arabian Sea upwelling were expected to intensify with global warming (Anderson et al., 2002; Gupta et al., 2003), since it was hypothesized that the Indian subcontinent would warm at a faster rate than the Indian Ocean, due to the larger heat capacity of oceans (Goes et al., 2005). However, in contrast to the original expectation, the recent study (Roxy et al., 2015; Swapna et al., 2017) reports weakening trends of the summer monsoon circulation over the Indian Ocean during the past 70 years (-0.30 ± 0.05 m sec^{-1}/decade; $r = -0.58$; $p < 0.01$; $n = 68$; Figure 1c). Besides, the northern Indian Ocean is warming more rapidly in the recent century than the Indian subcontinent (Figure 1, Roxy et al., 2014), which is also inconsistent with the original hypothesis (Anderson et al., 2002; Gupta et al., 2003). The observed trend of the monsoon circulations is considered to be due to the rapid/slow warming on the Indian Ocean/Indian subcontinent (Roxy et al., 2015). The weakening of the monsoon circulations over the Indian Ocean possibly results in a weakening of the Arabian Sea upwelling. However, a lack of reliable observational data limits understanding of recent and historical changes of the Arabian Sea upwelling. Direct observations of the Arabian Sea upwelling are scarce prior to the satellite era, and political instability in surrounding countries currently hinders continuous monitoring of the Arabian Sea upwelling. Reliable proxy data of the Arabian Sea upwelling would therefore significantly improve our understanding of the response of the SW monsoon and the Arabian Sea upwelling to the current anthropogenic warming.

Seawater oxygen isotopes ($\delta^{18}O_{sw}$, a hydrological tracer) in coral skeletons infered at a high-resolution (weekly to monthly) could provide reliable estimates of intra-seasonal oceanic processes like the Arabian Sea upwelling, since the Arabian Sea is located in an arid climate zone (rainfall <8 mm/month). Coral records at a high resolution allow us to separate the intra-seasonal signal from the annual cycle (e.g., Tudhope et al., 1996), which is an advantage compared to low-resolution proxy records that lack seasonal resolution. Here, we present various time-windows of $\delta^{18}O_{sw}$ records calculated from fossil and modern *Porites* corals, as an indicator for the Arabian Sea upwelling intensity during the past millennium. The coral records derive from the medieval climate anomaly (MCA), the little ice age (LIA), the mid-twentieth and the 21st century, and allow us to compare natural climate variability during the warm (cold) period of the last millennium with the recent changes resulting from anthropogenic warming.

2. Method

The coral samples were collected from Masirah Island (the Sultanate of Oman), a remote Island located in the Arabian Sea (>10 km off the Arabian peninsula; Figures S1 and S2). Our fossil corals were screened by X-ray diffraction analyses along the entire analytical paths at *ca*. 10 mm intervals and observing microstructures with scanning electron microscopy to assess potential diagenetic changes. Well-preserved samples

(Figure S3) were selected for geochemical analyses. U-Th age determinations (Shen et al., 2012) showed that the four fossil corals provided time windows from the past millennium: the MCA (1167 ± 4 CE), the LIA (1624 ± 28, 1703 ± 32 CE), and the mid-twentieth century (1968 ± 20 CE) (Table S1).

To obtain coral skeleton powder for geochemical analyses, 2 mm thick ledges were formed along the maximum axis of coral growth. The coral skeletal powders for Sr/Ca (a proxy for SST), oxygen isotopes ($\delta^{18}O_{coral}$: SST and $\delta^{18}O_{sw}$), and carbon isotopes ($\delta^{13}C_{coral}$: $\delta^{13}C$ in dissolved inorganic carbon, $\delta^{13}C_{DIC}$, and insolation) analyses were collected at 0.2–0.5 mm interval using a drill and a PC-controlled X-Y stage. The sampling intervals were determined to get biweekly resolution records (over 24 samples per year). $\delta^{18}O_{coral}$ and $\delta^{13}C_{coral}$ were analyzed using stable isotope ratio mass spectrometers installed at Hokkaido University. $\delta^{18}O_{coral}$ and $\delta^{13}C_{coral}$ in the modern coral were analyzed using 90–110 μg coral powders with a Finnigan MAT251 and Kiel II. $\delta^{18}O_{coral}$ and $\delta^{13}C_{coral}$ in the fossil corals were determined using 20–30 μg coral powders with a Finnigan MAT253 and Kiel IV. Sr/Ca was determined using an inductively coupled plasma optical emission spectrometer, Thermo scientific iCAP6200, installed at Hokkaido University. 90–110 μg of coral powder were dissolved in 25% nitric acid and diluted to a Ca concentration of 7 ppm with Milli-Q water (Watanabe et al., 2020). The precisions of Sr/Ca and $\delta^{18}O_{coral}$ were ±0.07%RSD and ±0.05‰$_{VPDB}$(1σ), respectively.

The age models for the modern coral records were developed using the maxima (winter/summer) and the minima (spring/autumn) of Sr/Ca values in any annual cycles as anchoring points, since SST showed the semi-annual cycle (seasonal cooling in both summer and winter) in the Arabian Sea (Figure S4). The anchoring points were tied to maxima (winter/summer) and minima (spring/autumn) of the OISST v2.1 (Banzon et al., 2020). A Sr/Ca ($\delta^{18}O_{coral}$)-SST dependency in the Arabian Sea was established using ordinary least squares regression based on the anchored data (Figure S5). For fossil coral records, we inserted time-series using Sr/Ca and carbon isotopes in coral skeletons ($\delta^{13}C_{coral}$). Seasonal maxima (minima) of Sr/Ca were tied to February 7th or August 3rd (May 21st or October 27th) as anchor points. We inserted time-series by assuming the equal growth rates between each anchoring point. We linearly interpolated to obtain biweekly resolution time series using the AnalySeries software, version 2.0.8 (Paillard et al., 1996).

We calculated $\delta^{18}O_{sw}$ records at a biweekly resolution based on paired measurements of Sr/Ca and $\delta^{18}O_{coral}$ using the centering method (Cahyarini et al., 2008), based on the assumption that contributions of SST and $\delta^{18}O_{sw}$ to $\delta^{18}O_{coral}$ were linear and constant through time. Centered values of Sr/Ca and $\delta^{18}O_{coral}$ (values relative to the mean for each specimen) were used for the $\delta^{18}O_{sw}$ estimation to avoid inter-colonial differences in mean values (Cahyarini et al., 2008). We used the slope of our Sr/Ca-SST dependency in the Arabian Sea and the slope value of the $\delta^{18}O_{coral}$-SST relationship (−0.18‰$_{VPDB}$/°C; Cahyarini et al., 2008; Gagan et al., 1998). The error of $\delta^{18}O_{sw}$ (1σ) was 0.06‰$_{VSMOW}$. Then, $\delta^{18}O_{sw}$ anomalies were calculated as values relative to the average $\delta^{18}O_{sw}$ in wintertime (November–April) after removing low-frequency variations (lower than 0.002 cycle/days) from the $\delta^{18}O_{sw}$ records. The $\delta^{18}O_{sw}$ anomalies in the SW monsoon season (May–October) were defined as summer $\delta^{18}O_{sw}$ reduction ($\delta^{18}O_{sw\text{-}reduc}$). We took the minimum values from the $\delta^{18}O_{sw\text{-}reduc}$ values (i.e., maximum reduction: max-$\delta^{18}O_{sw\text{-}reduc}$), as an indicator of the maximum Arabian Sea freshening in the SW monsoon season of any given year. The confidence intervals (CI) of max-$\delta^{18}O_{sw\text{-}reduc}$ in each coral were defined as 68th percentiles (1σ) which were estimated by a simple Monte-Carlo method (20,000 loops). The CI was combined with year-to-year changes of max-$\delta^{18}O_{sw\text{-}reduc}$ and the error of $\delta^{18}O_{sw}$. We tested the statistical significance of the differences in the max-$\delta^{18}O_{sw\text{-}reduc}$ using the bootstrap approach modified from Grothe et al. (2020) (Text S1). The statistical analyses were conducted using the R software (R Core Team, 2020)

3. Results and Discussions

3.1. Modern Coral Calibrations: Freshening of Surface Water Caused by the Arabian Sea Upwelling

The Sr/Ca record of the modern coral showed the semi-annual cycles typical for the Arabian Sea SST from 2009 to 2015 CE (Sr/Ca vs. SST: $r = -0.77$; $p < 0.01$; adjusted-$R^2 = 0.69$; $n = 157$) (Figures 2a and S5). The modern coral from Masirah Island recorded reductions of $\delta^{18}O_{sw}$ and $\delta^{13}C_{coral}$ in every SW monsoon season (Figures 2a and S4). For calibration, we compared the monthly coral $\delta^{18}O_{sw}$ record with monthly data of EN salinity (Good et al., 2013) and mixed layer depth (MLD: the depth with 0.8°C lower temperature compared to SST; Kara et al., 2000) measured by the Argo float system. The seasonality of coral $\delta^{18}O_{sw\text{-}reduc}$ reflected

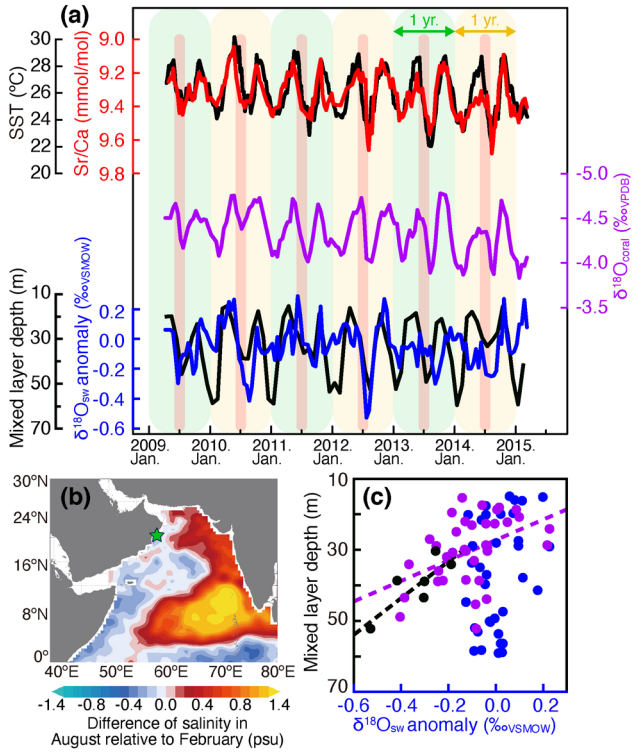

Figure 2. Modern coral records at a biweekly resolution from the Arabian Sea. (a) Sr/Ca (red line) and OISST v2.1 (black line, Banzon et al., 2020), $\delta^{18}O_{coral}$ (purple line), $\delta^{18}O_{sw}$ anomaly (blue line; values relative to the wintertime mean after detrending) and mixed layer depth measured by Argo float (black line). Yellow/green shadings indicate one year (January–December). Red shadings mark August. (b) Sea surface salinity anomalies in August 2013 relative to February 2014 (Aquarius OISSS; 1 × 1° grid). Note the freshening (blue colors) of the surface waters along the Somalian and the southern Arabian coast. Charts are computed with Live Access Server LAS8.6. The star indicates the sample site of our fossil and modern Arabian corals. (c) Scatter plot of mixed layer depth versus monthly $\delta^{18}O_{sw}$ anomalies and max-$\delta^{18}O_{sw\text{-}reduc}$ (purple: SW monsoon seasons, blue: winter months, black: max-$\delta^{18}O_{sw\text{-}reduc}$). The dotted black (purple) line: linear regression line of mixed layer depth versus max-$\delta^{18}O_{sw\text{-}reduc}$ ($\delta^{18}O_{sw}$ anomaly in the SW monsoon seasons).

the seasonal variation of salinity ($r = 0.79$, $p < 0.01$; adjusted-$R^2 = 0.59$; $n = 12$) (Figure S4). The coral $\delta^{18}O_{sw\text{-}reduc}$ negatively correlated with MLD in the SW monsoon season (from May to October; $\delta^{18}O_{sw\text{-}reduc}$ vs. MLD: $r = -0.44$; $p < 0.01$; adjusted-$R^2 = 0.17$; $n = 36$) (Figure 2c). There was a strong negative correlation between values of max-$\delta^{18}O_{sw\text{-}reduc}$ and MLD in August, that is, during the peak of the SW monsoon season (max-$\delta^{18}O_{sw\text{-}reduc}$ vs. MLD: $r = -0.82$; $p < 0.05$; adjusted-$R^2 = 0.59$; $n = 6$) (Figure 2c). The mean value of max-$\delta^{18}O_{sw\text{-}reduc}$ was $-0.31‰_{VSMOW}$ with CI [−0.36; −0.25] in the modern coral. However, the coral $\delta^{18}O_{sw}$ anomaly record weekly correlated with MLD in boreal winter (from November to April; $\delta^{18}O_{sw\text{-}anomaly}$ vs. MLD: $r = -0.26$; $p = 0.10$; adjusted-$R^2 = 0.05$; $n = 35$) (Figure 2c).

The calibration of the modern coral indicates that $\delta^{18}O_{sw\text{-}reduc}$ reflects a freshening and a deepening of MLD in the SW monsoon season along the coasts of Somalia and Oman driven by the Arabian Sea upwelling (Figures 2 and S6). In addition, max-$\delta^{18}O_{sw\text{-}reduc}$, that is, the maximum freshening in the SW monsoon season, reflects year-to-year variations of the Arabian Sea upwelling intensity. Coral $\delta^{18}O_{sw}$ agrees with *in situ* $\delta^{18}O_{sw}$ and salinity data of surface waters, which are significantly lower in the SW monsoon season than in boreal winter (Figures 2, S4 and S6). The low $\delta^{18}O_{sw}$ and freshening cannot be attributed to precipitation in the arid climate of Masirah Island (Figure S4). The Arabian Sea upwelling erodes the thermocline and mixes low-salinity water of the lower thermocline into surface waters, that is, MLD deepens. This results in a decrease of $\delta^{18}O_{sw}$ and the development of a uniform, low salinity profile down to 300 m depth in the SW monsoon season. The low-salinity seawater of the lower thermocline originates in the equatorial Indian Ocean and is transported to the Arabian Sea by the south-equatorial current and the coastal currents of eastern Africa and Somalia (Somali Current; upper 200 m depth) (Prasad & Ikeda, 2002; Schott & Fischer, 2000; Swallow et al., 1983). Reductions of $\delta^{18}O_{sw}$ in the SW monsoon season agree with those of $\delta^{13}C_{coral}$ which likely results from inflows of depleted- $^{13}C_{DIC}$ or an increase of turbidity by upwelling (Felis et al., 1998; Watanabe et al., 2017). The winter cooling and the dry winter monsoon cause the formation of high-density Arabian Sea water at the sea surface (Morrison et al., 1998; Schott & McCreary, 2001), that is, surface salinity (0–75 m) is higher than subsurface salinity in the Arabian Sea (Figure S6). The high-density surface water deepens MLD, but the surface water does not mix with the low salinity water from the lower thermocline.

3.2. Five Time-Windows of Coral Records: The Arabian Sea Upwelling During the Past Millennium

All fossil corals from Masirah Island recorded the semi-annual cycles of Sr/Ca, and reductions of coral $\delta^{18}O_{sw}$ and $\delta^{13}C_{coral}$ in the same season as seen in the modern coral (Figures 3a and S7). We developed time series of fossil coral proxy data by using Sr/Ca to determine the anchor points and $\delta^{13}C_{coral}$ to identify coral data from the SW monsoon. The five time-windows of modern and fossil corals covered 38 annual cycles in total (Figures 2 and 3). The mean of max-$\delta^{18}O_{sw\text{-}reduc}$ in the fossil corals was $-0.41‰_{VSMOW}$ with CI [−0.43; −0.38]. Values of max-$\delta^{18}O_{sw\text{-}reduc}$ in the modern coral were significantly higher than in the fossil corals (Text S1; Figures 3 and S8; $p < 0.05$; $n = 38$). Values of max-$\delta^{18}O_{sw\text{-}reduc}$ in the LIA (early LIA: $-0.40‰_{VSMOW}$ with CI [−0.45; −0.35]; middle-LIA: $-0.42‰_{VSMOW}$ with CI [−0.46; −0.37]) did not significantly differ from any other periods of the last millennium (MCA: −0.41 with CI [−0.45; −0.37]; mid-twentieth: −0.39 with CI [−0.43; −0.36]). Over the past millennium, max-$\delta^{18}O_{sw\text{-}reduc}$ positively correlated with various multi-proxy-based northern hemisphere temperature reconstructions ($r = 0.77$–0.96; $n = 5$) and the PAGES2k global

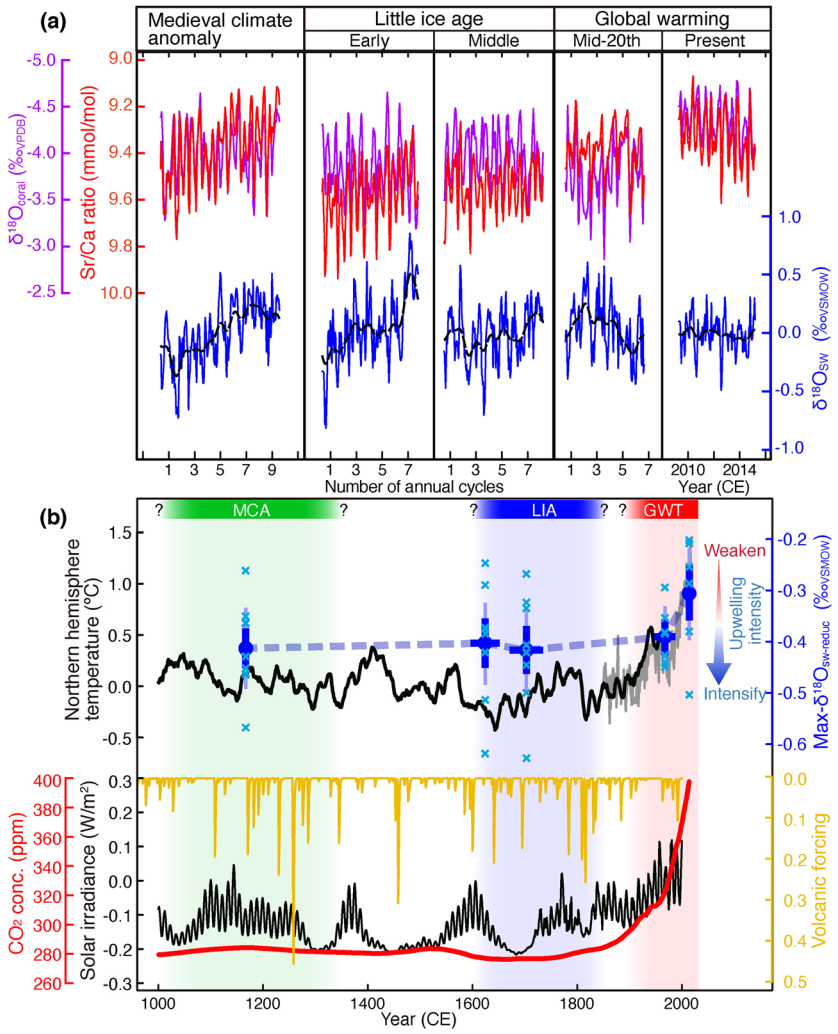

Figure 3. Modern and fossil coral records from the Arabian Sea. (a) Sr/Ca (red lines), $\delta^{18}O_{coral}$ (purple lines), and $\delta^{18}O_{sw}$ (blue lines). Black dotted lines indicate low-frequency variations of $\delta^{18}O_{sw}$ (bandpass filtered data). (b) Comparison of max-$\delta^{18}O_{sw\text{-}reduc}$ (minimum values of $\delta^{18}O_{sw\text{-}reduc}$) as a proxy for the intensity of the Arabian Sea upwelling, northern hemisphere temperature, and external climate forcing. Upper panel: max-$\delta^{18}O_{sw\text{-}reduc}$ (blue circles: mean values; blue and purple vertical bars: 68th and 90th percentiles of mean values; horizontal bars: errors of U-Th age; sky-blue crosses: individual values from each coral sample), and the northern hemisphere temperature relative to 1880–1900 CE (gray line: HadCRUT4 data; Jones et al., 2012; black line: multiproxy data, e.g., tree rings, sediment cores, ice cores; Hegerl et al., 2007). Lower panel: solar irradiation (black line: Schmidt et al., 2011), volcanic forcing (orange line; unitless; Toohey & Sigl, 2017), and atmospheric CO_2 concentrations (red line; Meinshausen et al., 2017).

temperature reconstruction ($r = 0.93$; $p < 0.05$; $n = 5$) (Figures 3b, S10 and S11) (Hegerl et al., 2007; Neukom et al., 2019).

$\delta^{18}O_{sw}$ of the fossil corals show seasonal cycles similar to the modern coral, with an intra-seasonal freshening in the SW monsoon season (Figure S7). Therefore, max-$\delta^{18}O_{sw\text{-}reduc}$ is used as an indicator of the Arabian Sea upwelling intensity during the past millennium (Figure 3b). The statistical test comparing the max-$\delta^{18}O_{sw\text{-}reduc}$ values of modern and fossil corals indicates that the Arabian Sea upwelling is significantly weaker at present than in the last millennium (95% confidence level). This significant difference in the max-$\delta^{18}O_{sw\text{-}reduc}$ does not randomly arise from the process of reconstruction using the short coral records (Text S1 and Figure S8). However, the last millennium, that is, the period before the global warming onset, was an era with a stable intensity of the Arabian Sea upwelling, as the max-$\delta^{18}O_{sw\text{-}reduc}$ values in the LIA are very similar to those in the MCA. The current weakening of Arabian Sea upwelling inferred from our corals is consistent with the weakening trends of the wind stress curl (i.e., upwelling forcing; FNMOC data

set) and the Indian monsoon circulation index in the past 50 and 70 years ($-0.084 \pm 0.017 \times 10^{-6}$ N × m^{-3}/decade; $r = -0.56$; $p < 0.01$, $n = 53$; -0.30 ± 0.05 m × sec^{-1}/decade; $r = -0.58$; $p < 0.01$; $n = 68$) (Swapna et al., 2017). In addition, the current wind stress curl is significantly weaker than during the mid-twentieth century ($p < 0.05$) (Text S1 and Figure S8). The current weakening of Arabian Sea upwelling would also be supported by a decrease of primary productivity along the southern Arabian coast for the past decades (Roxy et al., 2016). The increase of max-$\delta^{18}O_{sw\text{-}reduc}$ in recent years could not be explained by an increase of salinity in the source of the Arabian Sea subsurface water during the past century. Coral $\delta^{18}O_{sw}$ records from the south-equatorial Indian Ocean show a trend toward more negative $\delta^{18}O_{sw}$/less saline water during the past century (Figure S12; Pfeiffer et al., 2019; Zinke et al., 2008). This freshening in the south-equatorial Indian Ocean is consistent with the expansion and freshening of the Indo-Pacific warm pool observed since the 1950s. We note, however, that our coral record does not agree with proxy data from the Arabian Sea sediment cores (populations of *Globigerina bulloides*) (Figure S13) (Anderson et al., 2002; Gupta et al., 2003). The records from the sediment cores suggest pronounced variations of the Arabian Sea upwelling during the past millennium and an intensification since the seventeenth century. There is no instrumental or proxy-based evidence that supports the trend of *G. bulloides* populations from the little ice age to 1986 CE (Anderson et al., 2002; Fleitmann et al., 2004; Roxy et al., 2016; Swapna et al., 2017; Zinke et al., 2009). The discrepancies between the corals and the sediment core records could be due to the poor age control and the low temporal resolution (13–38 years/data point) of sediment cores (Text S2 and Figure S13).

The current weakening of Arabian Sea upwelling likely results from the weakening of the SW monsoon due to anthropogenic forcing. The land-sea thermal gradient is declining in the recent century due to the faster warming on the northern Indian Ocean compared to the Indian subcontinent (Figure 1) (Chung & Ramanathan, 2006; Ramanathan et al., 2005; Roxy et al., 2014, 2015). The rapid warming in the northwestern Indian Ocean is more pronounced in the SW monsoon season (1.02 ± 0.02°C/century; $r = 0.97$; $p < 0.01$, $n = 140$) compared to the winter (0.79 ± 0.02°C/century; $r = 0.95$; $p < 0.01$, $n = 140$; Figure 1b). This rapid warming of the northwestern Indian Ocean during the past century highly correlates with the greenhouse-gas-induced warming of the northern hemisphere (field correlation analysis; $r > 0.8$; $p < 0.1$; Figure S14) (Alory & Meyers, 2009). While a causal link between the recent northern hemisphere warming and the Indian Ocean warming is currently under investigation (Naidu et al., 2020; Roxy et al., 2014), anthropogenic forcing plays an important role (Alory & Meyers, 2009). In contrast to the northern Indian Ocean, anthropogenic aerosol emissions over South Asia may absorb solar irradiation and slow the current warming over the Indian subcontinent (0.24 ± 0.03°C/century; $r = 0.53$; $p < 0.01$, $n = 140$; Figure 1; Ramanathan et al., 2005). As our corals suggest, although the intensity of Arabian Sea upwelling fluctuates inversely with the northern hemisphere and global mean temperatures (Figure 3b), the recent weakening of Arabian Sea upwelling is much more pronounced compared to the changes from the MCA to the LIA (Figure 3b). The current asymmetric warming due to anthropogenic forcing (emissions of greenhouse gases and aerosols) would appear to have a stronger impact on the SW monsoon and the Arabian Sea upwelling than temperature changes due to natural forcing (Figure 3b; volcanic eruptions; insolation, Anchukaitis et al., 2017; Neukom et al., 2019) during the last millennium.

4. Conclusions

Our modern and fossil corals from Masirah Island provide the first direct evidence that the Arabian Sea upwelling was stable during the last millennium and significantly weakens during the current anthropogenic warming. The reduction of the land-sea thermal contrast due to the faster warming of the northern Indian Ocean compared to the Indian subcontinent likely weakens the SW monsoon and the Arabian Sea upwelling. Our findings imply that the Arabian Sea upwelling will likely continue to weaken during the current and future anthropogenic warming with important climatic (e.g., SST, monsoon rainfall, sea level, and primary productions) and socioeconomic (e.g., agricultural productions, and fisheries) impacts.

Data Availability Statement

All coral data are available on the data repository at KIKAI Institute for coral reef sciences (https://coralogy.kikaireefs.org/C-1%20Scientific%20data.html)

Acknowledgments
The authors acknowledge K. Ohmori for his help with fieldwork in the Sultanate of Oman. H. Nomura and K. Nakamura helped to slice the fossil corals. T. Tajima assisted with scanning electron microscopy observations and X-ray diffraction analysis. The authors acknowledge T. Irino for managing MAT253 and Kiel-IV. T.-L.Yu organized U-Th lab at National Taiwan University. This work was supported by JSPS KAKENHI Grant Number JP25257207. U-Th dating was supported was supported by grants from the Science Vanguard Research Program of the Ministry of Science and Technology (MOST) (109-2123-M-002-001 to C.-C. Shen), the National Taiwan University (109L8926 to C.-C. Shen), the Higher Education Sprout Project of the Ministry of Education, Taiwan ROC (109L901001 to C.-C. Shen). All authors declare that they have no competing interest.

References

Alory, G., & Meyers, G. (2009). Warming of the upper equatorial Indian Ocean and changes in the heat budget (1960–99). *Journal of Climate*, *22*(1), 93–113. https://doi.org/10.1175/2008JCLI2330.1

Anchukaitis, K. J., Wilson, R., Briffa, K. R., Büntgen, U., Cook, E. R., D'Arrigo, R., et al. (2017). Last millennium Northern Hemisphere summer temperatures from tree rings: Part II, spatially resolved reconstructions. *Quaternary Science Reviews*, *163*, 1–22. https://doi.org/10.1016/j.quascirev.2017.02.020

Anderson, D. M., Overpeck, J. T., & Gupta, A. K. (2002). Increase in the Asian southwest monsoon during the past four centuries. *Science*, *297*(5581), 596–599. https://doi.org/10.1126/science.1072881

Banzon, V., Smith, T. M., Steele, M., Huang, B., & Zhang, H.-M. (2020). Improved estimation of proxy sea surface temperature in the Arctic. *Journal of Atmospheric and Oceanic Technology*, *37*(2), 341–349. https://doi.org/10.1175/JTECH-D-19-0177.1

Barber, R. T., Marra, J., Bidigare, R. C., Codispoti, L. A., Halpern, D., Johnson, Z., et al. (2001). Primary productivity and its regulation in the Arabian Sea during 1995. *Deep-Sea Research Part II: Topical Studies in Oceanography*, *48*. https://doi.org/10.1016/S0967-0645(00)00134-X

Brock, J. C., & McClain, C. R. (1992). Interannual variability in phytoplankton blooms observed in the northwestern Arabian Sea during the southwest monsoon. *Journal of Geophysical Research*, *97*(C1), 733. https://doi.org/10.1029/91JC02225

Cahyarini, S. Y., Pfeiffer, M., Timm, O., Dullo, W.-C., & Schönberg, D. G. (2008). Reconstructing seawater $\delta^{18}O$ from paired coral $\delta^{18}O$ and Sr/Ca ratios: Methods, error analysis and problems, with examples from Tahiti (French Polynesia) and Timor (Indonesia). *Geochimica et Cosmochimica Acta*, *72*(12), 2841–2853. https://doi.org/10.1016/j.gca.2008.04.005

Chung, C. E., & Ramanathan, V. (2006). Weakening of north Indian SST gradients and the monsoon rainfall in India and the Sahel. *Journal of Climate*, *19*(10), 2036–2045. https://doi.org/10.1175/JCLI3820.1

Felis, T., Pätzold, J., Loya, Y., & Wefer, G. (1998). Vertical water mass mixing and plankton blooms recorded in skeletal stable carbon isotopes of a Red Sea coral. *Journal of Geophysical Research*, *103*(13), 30731–30739. https://doi.org/10.1029/98JC02711

Fleitmann, D., Burns, S. J., Neff, U., Mudelsee, M., Mangini, A., & Matter, A. (2004). Paleoclimatic interpretation of high-resolution oxygen isotope profiles derived from annually laminated speleothems from Southern Oman. *Quaternary Science Reviews*, *23*(7–8), 935–945. https://doi.org/10.1016/j.quascirev.2003.06.019

Gagan, M. K., Ayliffe, L. K., Hopley, D., Cali, J. A., Mortimer, G. E., Chappell, J., et al. (1998). Temperature and Surface-Ocean Water Balance of the Mid-Holocene Tropical Western Pacific. *Science*, *279*(5353), 1014–1018. https://doi.org/10.1126/science.279.5353.1014

Goes, J. I., Thoppil, P. G., Gomes, H. D. R., & Fasullo, J. T. (2005). Warming of the Eurasian landmass is making the Arabian sea more productive. *Science*, *308*(5721), 545–547. https://doi.org/10.1126/science.1106610

Good, S. A., Martin, M. J., & Rayner, N. A. (2013). EN4: Quality controlled ocean temperature and salinity profiles and monthly objective analyses with uncertainty estimates. *Journal of Geophysical Research: Oceans*, *118*, 6704–6716. https://doi.org/10.1002/2013JC009067

Grothe, P. R., Cobb, K. M., Liguori, G., Di Lorenzo, E., Capotondi, A., Lu, Y., et al. (2020). Enhanced El Niño-Southern Oscillation Variability in Recent Decades. *Geophysical Research Letters*, *47*(7). https://doi.org/10.1029/2019GL083906

Gupta, A. K., Anderson, D. M., & Overpeck, J. T. (2003). Abrupt changes in the Asian southwest monsoon during the Holocene and their links to the North Atlantic Ocean. *Nature*, *421*(6921), 354–357. https://doi.org/10.1038/nature01340

Hansen, J., Ruedy, R., Sato, M., & Lo, K. (2010). Global surface temperature change. *Reviews of Geophysics*, *48*(4). RG4004. https://doi.org/10.1029/2010RG000345

Hegerl, G. C., Crowley, T. J., Allen, M., Hyde, W. T., Pollack, H. N., Smerdon, J., & Zorita, E. (2007). Detection of human influence on a new, validated 1500-year temperature reconstruction. *Journal of Climate*, *20*(4), 650–666. https://doi.org/10.1175/JCLI4011.1

Izumo, T., Montégut, C. B., Luo, J.-J., Behera, S. K., Masson, S., & Yamagata, T. (2008). The role of the Western Arabian Sea upwelling in Indian monsoon rainfall variability. *Journal of Climate*, *21*(21), 5603–5623. https://doi.org/10.1175/2008JCLI2158.1

Jones, P. D., Lister, D. H., Osborn, T. J., Harpham, C., Salmon, M., & Morice, C. P. (2012). Hemispheric and large-scale land-surface air temperature variations: An extensive revision and an update to 2010. *Journal of Geophysical Research*, *117*. https://doi.org/10.1029/2011JD017139

Kara, A. B., Rochford, P. A., & Hurlburt, H. E. (2000). An optimal definition for ocean mixed layer depth. *Journal of Geophysical Research*, *105*, 16803–16821. https://doi.org/10.1029/2000JC900072

Krishna Kumar, K., Rupa Kumar, K., Ashrit, R. G., Deshpande, N. R., & Hansen, J. W. (2004). Climate impacts on Indian agriculture. *International Journal of Climatology*, *24*(11), 1375–1393. https://doi.org/10.1002/joc.1081

Meinshausen, M., Vogel, E., Nauels, A., Lorbacher, K., Meinshausen, N., Etheridge, D. M., et al. (2017). Historical greenhouse gas concentrations for climate modeling (CMIP6). *Geoscientific Model Development*, *10*(5), 2057–2116. https://doi.org/10.5194/gmd-10-2057-2017

Morrison, J. M., Codispoti, L. A., Gaurin, S., Jones, B., Manghnani, V., & Zheng, Z. (1998). Seasonal variation of hydrographic and nutrient fields during the US JGOFS Arabian Sea process study. *Deep Sea Research Part II: Topical Studies in Oceanography*, *45*, 2053–2101. https://doi.org/10.1016/S0967-0645(98)00063-0

Naidu, P. D., Ganeshram, R., Bollasina, M. A., Panmei, C., Nürnberg, D., & Donges, J. F. (2020). Coherent response of the indian monsoon rainfall to Atlantic multi-decadal variability over the last 2000 years. *Scientific Reports*, *10*(1), 1302. https://doi.org/10.1038/s41598-020-58265-3

Neukom, R., Barboza, L. A., Erb, M. P., Shi, F., Emile-Geay, J., Evans, M. N., et al. (2019). Consistent multidecadal variability in global temperature reconstructions and simulations over the Common Era. *Nature Geoscience*, *12*(8), 643–649. https://doi.org/10.1038/s41561-019-0400-0

Paillard, D., Labeyrie, L., & Yiou, P. (1996). Macintosh Program performs time-series analysis. *Eos Transactions American Geophysical Union*, *77*(39). https://doi.org/10.1029/96eo00259

Pfeiffer, M., Reuning, L., Zinke, J., Garbe-Schönberg, D., Leupold, M., & Dullo, W. C. (2019). 20th century $\delta^{18}O$ seawater and salinity variations reconstructed from paired $\delta^{18}O$ and Sr/Ca measurements of a La reunion coral. *Paleoceanography and Paleoclimatology*, *34*(12), 2183–2200. https://doi.org/10.1029/2019PA003770

Prasad, T. G., & Ikeda, M. (2002). A numerical study of the seasonal variability of Arabian Sea high-salinity water. *Journal of Geophysical Research*, *107*. https://doi.org/10.1029/2001jc001139

Ramanathan, V., Chung, C., Kim, D., Bettge, T., Buja, L., Kiehl, J. T., et al. (2005). Atmospheric brown clouds: Impacts on South Asian climate and hydrological cycle. *Proceedings of the National Academy of Sciences*, *102*(15), 5326–5333. https://doi.org/10.1073/pnas.0500656102

R Core Team. (2020). *R: A language and environment for statistical computing*. R Foundation for Statistical Computing. Retrieved from https://www.R-project.org/

Roxy, M. K., Modi, A., Murtugudde, R., Valsala, V., Panickal, S., Prasanna Kumar, S., et al. (2016). A reduction in marine primary productivity driven by rapid warming over the tropical Indian Ocean. *Geophysical Research Letters*, *43*(2), 826–833. https://doi.org/10.1002/2015GL066979

Roxy, M. K., Ritika, K., Terray, P., & Masson, S. (2014). The curious case of Indian Ocean warming. *Journal of Climate*, *27*(22), 8501–8509. https://doi.org/10.1175/JCLI-D-14-00471.1

Roxy, M. K., Ritika, K., Terray, P., Murtugudde, R., Ashok, K., & Goswami, B. N. (2015). Drying of Indian subcontinent by rapid Indian ocean warming and a weakening land-sea thermal gradient. *Nature Communications*, *6*, 1–10. https://doi.org/10.1038/ncomms8423

Schmidt, G. A., Jungclaus, J. H., Ammann, C. M., Bard, E., Braconnot, P., Crowley, T. J., et al. (2011). Climate forcing reconstructions for use in PMIP simulations of the last millennium (v1.0). *Geoscientific Model Development*, *4*(1), 33–45. https://doi.org/10.5194/gmd-4-33-2011

Schott, F. A., & Fischer, J. (2000). Winter monsoon circulation of the northern Arabian Sea and Somali Current. *Journal of Geophysical Research*, *105*, 6359–6376. https://doi.org/10.1029/1999JC900312

Schott, F. A., & McCreary, J. P. (2001). The monsoon circulation of the Indian Ocean. *Progress in Oceanography*, *51*(1), 1–123. https://doi.org/10.1016/S0079-6611(01)00083-0

Shen, C.-C., Wu, C.-C., Cheng, H., Lawrence Edwards, R., Hsieh, Y.-T., Gallet, S., et al. (2012). High-precision and high-resolution carbonate 230Th dating by MC-ICP-MS with SEM protocols. *Geochimica et Cosmochimica Acta*, *99*, 71–86. https://doi.org/10.1016/j.gca.2012.09.018

Swallow, J. C., Molinari, R. L., Bruce, J. G., Brown, O. B., & Evans, R. H. (1983). Development of near-surface flow pattern and water mass distribution in the Somali Basin in response to the southwest monsoon of 1979. *Journal of Physical Oceanography*, *13*, 1398–1415. https://doi.org/10.1175/1520-0485(1983)013<1398:DONSFP>2.0.CO;2

Swapna, P., Jyoti, J., Krishnan, R., Sandeep, N., & Griffies, S. M. (2017). Multidecadal weakening of indian summer monsoon circulation induces an increasing northern Indian Ocean sea level. *Geophysical Research Letters*, *44*(20), 10560–10572. https://doi.org/10.1002/2017GL074706

Toohey, M., & Sigl, M. (2017). Volcanic stratospheric sulfur injections and aerosol optical depth from 500 BCE to 1900 CE. *Earth System Science Data*, *9*(2), 809–831. https://doi.org/10.5194/essd-9-809-2017

Tudhope, A. W., Lea, D. W., Shimmield, G. B., Chilcott, C. P., & Head, S. (1996). Monsoon climate and Arabian Sea coastal upwelling recorded in massive corals from Southern Oman. *PALAIOS*, *11*(4), 347. https://doi.org/10.2307/3515245

Watanabe, T. K., Watanabe, T., Ohmori, K., & Yamazaki, A. (2020). Improving analytical method of Sr/Ca ratios in coral skeletons for paleo- SST reconstructions using ICP-OES. *Limnology and Oceanography: Methods*, *18*, 297–310. https://doi.org/10.1002/lom3.10357

Watanabe, T. K., Watanabe, T., Yamazaki, A., Pfeiffer, M., Garbe-Schönberg, D., & Claereboudt, M. R. (2017). Past summer upwelling events in the Gulf of Oman derived from a coral geochemical record. *Scientific Reports*, *7*(1), 1–7. https://doi.org/10.1038/s41598-017-04865-5

Webster, P. J., & Yang, S. (1992). Monsoon and ENSO: Selectively interactive systems. *Quarterly Journal of the Royal Meteorological Society*, *118*, 877–926. https://doi.org/10.1002/qj.49711850705

Wu, G., Liu, Y., He, B., Bao, Q., Duan, A., & Jin, F.-F. (2012). Thermal controls on the asian summer monsoon. *Scientific Reports*, *2*, 1–7. https://doi.org/10.1038/srep00404

Zinke, J., Pfeiffer, M., Timm, O., Dullo, W.-C., & Brummer, G. J. A. (2009). Western Indian Ocean marine and terrestrial records of climate variability: A review and new concepts on land-ocean interactions since AD 1660. *International Journal of Earth Sciences*, *98*(1), 115–133. https://doi.org/10.1007/s00531-008-0365-5

Zinke, J., Pfeiffer, M., Timm, O., Dullo, W.-C., Kroon, D., & Thomassin, B. A. (2008). Mayotte coral reveals hydrological changes in the western Indian Ocean between 1881 and 1994. *Geophysical Research Letters*, *35*(23). L23707. https://doi.org/10.1029/2008GL035634

References From the Supporting Information

Boyer, T. P., Antonov, J. I., Baranova, O. K., Garcia, H. E., Johnson, D. R., Mishonov, A. V., et al. (2013). *World ocean database 2013*. https://doi.org/10.7289/V5NZ85MT

Cheung, A., Fox-Kemper, B., & Herbert, T. (2019). Can we use sea surface temperature and productivity proxy records to reconstruct Ekman upwelling? *Climate of the Past*, *15*(6), 1985–1998. https://doi.org/10.5194/cp-15-1985-2019

D'Arrigo, R., Wilson, R., & Jacoby, G. (2006). On the long-term context for late twentieth century warming. *Journal of Geophysical Research*, *111*(3), 1–12. https://doi.org/10.1029/2005JD006352

Felis, T., Lohmann, G., Kuhnert, H., Lorenz, S. J., Scholz, D., Pätzold, J., et al. (2004). Increased seasonality in Middle East temperatures during the last interglacial period. *Nature*, *429*(6988), 164–168. https://doi.org/10.1038/nature02546

Kalnay, E., Kanamitsu, M., Kistler, R., Collins, W., Deaven, D., Gandin, L., et al. (1996). The NCEP/NCAR 40-year reanalysis project. *Bulletin of the American Meteorological Society*, *77*(3), 437–471. https://doi.org/10.1175/1520-0477(1996)077<0437:TNYRP>2.0.CO;2

Mann, M. E., Zhang, Z., Hughes, M. K., Bradley, R. S., Miller, S. K., Rutherford, S., & Ni, F. (2008). Proxy-based reconstructions of hemispheric and global surface temperature variations over the past two millennia. *Proceedings of the National Academy of Sciences*, *105*(36), 13252–13257. https://doi.org/10.1073/pnas.0805721105

Moberg, A., Sonechkin, D. M., Holmgren, K., Datsenko, N. M., & Karlén, W. (2005). Highly variable Northern Hemisphere temperatures reconstructed from low- and high-resolution proxy data. *Nature*, *433*(7026), 613–617. https://doi.org/10.1038/nature03265

Nurhati, I. S., Cobb, K. M., & Di Lorenzo, E. (2011). Decadal-scale SST and salinity variations in the central tropical Pacific: Signatures of natural and anthropogenic climate change. *Journal of Climate*, *24*(13), 3294–3308. https://doi.org/10.1175/2011JCLI3852.1

Otto-Bliesner, B. L., Brady, E. C., Fasullo, J., Jahn, A., Landrum, L., Stevenson, S., et al. (2016). Climate variability and change since 850 CE: An ensemble approach with the community earth system model. *Bulletin of the American Meteorological Society*, *97*(5), 735–754. https://doi.org/10.1175/BAMS-D-14-00233.1

Pfeiffer, M., Timm, O., Dullo, W.-C., & Podlech, S. (2004). Oceanic forcing of interannual and multidecadal climate variability in the southwestern Indian Ocean: Evidence from a 160-year coral isotopic record (La Réunion, 55°E, 21°S). *Paleoceanography*, *19*(4). https://doi.org/10.1029/2003PA000964

Reynolds, R. W., Rayner, N. A., Smith, T. M., Stokes, D. C., & Wang, W. (2002). An improved in situ and satellite SST analysis for climate. *Journal of Climate*, *15*(13), 1609–1625. https://doi.org/10.1175/1520-0442(2002)015<1609:AIISAS>2.0.CO;2

Rodionov, S. N. (2004). A sequential algorithm for testing climate regime shifts. *Geophysical Research Letters*, *31*(9). https://doi.org/10.1029/2004GL019448

Sagar, N., Hetzinger, S., Pfeiffer, M., Masood Ahmad, S., Dullo, W. C., & Garbe-Schönberg, D. (2016). High-resolution Sr/Ca ratios in a Porites lutea coral from Lakshadweep Archipelago, southeast Arabian Sea: An example from a region experiencing steady rise in the reef temperature. *Journal of Geophysical Research: Oceans*, *121*(1), 252–266. https://doi.org/10.1002/2015JC010821

Schmidt, G. A. (1999). Forward modeling of carbonate proxy data from planktonic foraminifera using oxygen isotope tracers in a global ocean model. *Paleoceanography*, *14*(4), 482–497. https://doi.org/10.1029/1999PA900025

Schneider, L., Smerdon, J. E., Büntgen, U., Wilson, R. J. S., Myglan, V. S., Kirdyanov, A. V., & Esper, J. (2015). Revising midlatitude summer temperatures back to A.D. 600 based on a wood density network. *Geophysical Research Letters*, *42*(11), 4556–4562. https://doi.org/10.1002/2015GL063956

Shi, F., Li, J., & Wilson, R. J. S. (2014). A tree-ring reconstruction of the South Asian summer monsoon index over the past millennium. *Scientific Reports*, *4*, 1–8. https://doi.org/10.1038/srep06739

Wilson, R., Anchukaitis, K., Briffa, K. R., Büntgen, U., Cook, E., D'Arrigo, R., et al. (2016). Last millennium northern hemisphere summer temperatures from tree rings: Part I: The long term context. *Quaternary Science Reviews*, *134*, 1–18. https://doi.org/10.1016/j.quascirev.2015.12.005

Zinke, J., Dullo, W.-C., Heiss, G. A., & Eisenhauer, A. (2004). ENSO and Indian Ocean subtropical dipole variability is recorded in a coral record off southwest Madagascar for the period 1659 to 1995. *Earth and Planetary Science Letters*, *228*(1–2), 177–194. https://doi.org/10.1016/j.epsl.2004.09.028